MRI Volumetric Analysis of Multiple Sclerosis: Methodology and Validation

Lihong Li, *Member, IEEE*, Xiang Li, Hongbing Lu, *Member, IEEE*, Wei Huang, Christopher Christodoulou, Alina Tudorica, Lauren B. Krupp, and Zhengrong Liang, *Member, IEEE*

***Abstract*—We present an automatic mixture-based algorithm for segmentation of brain tissues (white and gray matters—WM and GM), cerebral spinal fluid (CSF), and brain lesions to quantitatively analyze multiple sclerosis. The method performs intensity-based tissue classification using multispectral magnetic resonance (MR) images based on a stochastic model. With the existence of white Gaussian noise and spatially invariant blurring in acquired MR images, a Karhunen–Loéve (K–L) domain Wiener filter is applied for accurate noise reduction and resolution restoration on blurred and noisy images to minimize the partial volume effect (PVE), which is a major limiting factor for the quantitative analysis. Following that, we utilize a Markov random field Gibbs model to integrate the local spatial information into the well-established expectation-maximization model-fitting algorithm. Each voxel is then classified by a maximum *a posterior* (MAP) criterion, indicating its probabilities of belonging to each class, i.e., each voxel is labeled as a mixel with different tissue percentages, leading to further minimization of the PVE. The volumes of WM, GM, CSF, and brain lesions are extracted from the mixture-based segmentation and the corresponding brain atrophies are computed. In this study, we have investigated the accuracy and repeatability of the algorithm with inclusion of noise analysis and point spread function for image resolution enhancement. Experimental results on phantom, healthy volunteer, and patient studies are presented.**

***Index Terms*—Markov random field, mixture, MRI, multispectral, partial volume effect, segmentation.**

I. Introduction

MULTIPLE SCLEROSIS (MS) is a chronic, immune-mediated, demyelinating disease that affects the central nervous system [1]. Approximately 80 to 100 per 100 000 people have MS in the United States, making it the most frequent cause of disability in early to middle adulthood other than trauma [2]. Quantitative analysis of white matter (WM), gray matter (GM), cerebral spinal fluid (CSF), as well as brain lesion provides a means for establishing a parametric index for evaluation of MS burden [3]. Longitudinal evaluation of change in the parametric index using a systematic segmentation approach provides a useful, objective measure of the effect of MS therapeutic interventions.

Magnetic resonance imaging (MRI) is an appealing surrogate in the study of MS, as MRI changes reflect the pathology of the disease [4]. With current fast MRI techniques, a set of multispectral images can be acquired rapidly, including T_1 and T_2 relaxation time, proton density weighted, and fluid attenuated inversion recovery (FLAIR) [5], [6]. Because these images are spatially registered over the three-dimensional (3-D) space, information extracted by means of image processing from multispectral images is obviously more valuable than that extracted from each image individually [7]. A number of methods have been proposed for the segmentation of multispectral MR images [7]–[11]. Few studies have been reported to measure central cerebral atrophy (CCA) with correlation study on clinical findings [12]. To the best of our knowledge, very few repeatability evaluations on quantification in a longitudinal study have been reported. In order to develop a clinically accepted tool for a longitudinal study, the accuracy and repeatability of the algorithm must be validated. Miller, *et al.* also pointed out that brain lesions are inherently fuzzy with "soft" rather than "hard" boundaries [13]. Therefore, segmenting each voxel as a mixel with different tissue percentages is theoretically attractive and clinically desirable to minimize the partial volume effects (PVE) among the tissue boundaries.

Taking these facts into account, we have proposed a mixture-based maximum *a posterior* probability expectation-maximization (MAP-EM) segmentation framework for quantification of tissue components inside each voxel [14]. Unlike the work of Zhang, *et al.* [15], where spatial information was integrated into a MAP-EM algorithm for voxel labels, not mixtures, in this paper we further extend the MAP-EM framework for multispectral MR images to achieve a mixture-based segmentation for accurate and robust performance. We also integrated the noise analysis and point spread function (PSF) into our framework. A mixture-based quantification of brain volumes has been performed in a longitudinal clinical study.

In the following, our MAP-EM framework is presented with validation by both accuracy and repeatability measures on phantom, healthy volunteer, and patient studies.

II. Materials and Methods

A. MRI Acquisition

MRI sessions were performed using a 1.5 Tesla Philips Edge whole-body scanner with a body coil as the transmitter and

Manuscript received December 5, 2002; revised June 20, 2003. This work was supported in part by the National Institutes of Health Grant #CA82402 and the National Multiple Sclerosis Society Grant #RG3042-A-2.

L. Li is with the Electrical Engineering and Radiology Departments, State University of New York, Stony Brook, NY 11794 USA (e-mail: lli@mil.sunysb.edu).

X. Li, H. Lu, W. Huang, and A. Tudorica are with the Radiology Department, State University of New York, Stony Brook, NY 11794 USA.

C. Christodoulou and L. B. Krupp are with the Neurology Department, State University of New York, Stony Brook, NY 11794 USA.

Z. Liang is with the Radiology and Computer Science Departments, State University of New York, Stony Brook, NY 11794 USA.

Digital Object Identifier 10.1109/TNS.2003.817334

a birdcage head coil as the receiver. A 3-D spoiled gradient-recalled (SPGR) sequence [5], [6] was employed to acquire T_1-weighted axial images covering the whole brain with 30° flip angle, $T_E = 5$ ms, $T_R = 30$ ms, 1.5 mm slice thickness, 24 cm field-of-view (FOV), and 256 × 256 matrix size. A 3-D extended phase conjugate symmetry rapid spin echo sequence (EXPRESS) with fat suppression [5], [6] was used to collect T_2-weighted axial images with the same acquisition location and parameters, except for $T_E = 95$ ms, $T_R = 4000$ ms, and ETL = 136. A FLAIR image with CSF saturation was also acquired from each patient with the same location and FOV in the sessions. The total MRI scanning time was less than 40 min. These three scans were performed sequentially with the subject lying in the same position in the coil. The multispectral images were registered well in the spatial domain.

B. Fourier Domain Interpolation for Isotropic Voxel Size

MR images were acquired with a square pixel size but with variable thickness, resulting in a noncubic voxel size. In our study, the slice thickness of the constructed images is 1.5 mm, which is larger than the pixel size (0.9375×0.9375 mm^2) in the X–Y plane. Therefore, a Fourier domain-based interpolation by zero padding was first applied to the data sets for constructing an equal distance for local intensity vector selection in the 3-D spatial domain [16]. This procedure was applied to all multispectral images.

C. K–L Wiener Restoration of Blurred and Noisy Images

MR image datasets include a spatially invariant blurring, which can be characterized by the PSF. Deblurring is desired to improve the quantitative analysis, but usually at the cost of noise. Therefore, noise suppression must be considered. MRI noise can be modeled as white Gaussian, embedded in the in-phase and quadrature components of the received signal [17].

For data contaminated with white Gaussian noise and spatially invariant blurring, Wiener restoration is an optimal solution based on the minimum least-square criterion for a linear system. With further consideration of the correlation among the multispectral images, we employed the Karhunen–Loéve (K–L) transform strategy for an improved noise treatment [18]. Then the K–L domain Wiener restoration has the form of

$$\hat{\breve{Y}}_i(u, v) = \frac{H_c(u, v)\breve{Y}_i(u, v)}{|H_c(u, v)| + \sigma_n^2/\Phi_{\breve{Y}}(u, v)} \tag{1}$$

where $\Phi_{\breve{Y}}$ is the power spectrum of K–L transformed image $\breve{y}_i$ at slice i and (u, v) denotes the 2-D Fourier transform (FT) coordinates. The system matrix H_c describes the blurring kernel in each individual slice [19]. By taking both the spatial correlation and noise/blurring properties into account, the K–L domain Wiener filtering provides a theoretically-based restoration of the blurred and noisy image.

D. Mixture-Based Segmentation Algorithm

Conventionally, an image is classified by labels and each voxel is assigned a label, which reflects the main property of that voxel. As the voxel size increases, quantitative analysis error appears due to the PVE among different tissues. Therefore, we proposed an optimal solution for the PVE, i.e., a mixture-based segmentation for quantification of those tissue components inside each voxel.

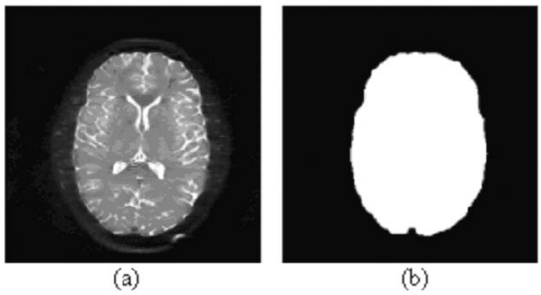

Fig. 1. (a) A slice of the T_2-weighted image. (b) The extracted brain mask corresponding to the ICV.

We first applied a fully automated fast self-adaptive online vector quantization (SOVQ) segmentation [20] to extract the intra-cranial volume (ICV) as a brain mask from the T_2-weighted image. Fig. 1(a) shows a slice of the T_2-weighted image of a volunteer, which has a good contrast between CSF and brain tissues. Fig. 1(b) shows the extracted brain mask corresponding to the ICV. Following that, we applied the SOVQ segmentation again to assign labels to those tissue types within the ICV. From these labels, we computed the initial parameter estimations for our iterative mixture-based segmentation algorithm, as described below.

The algorithm iteratively estimates the model parameters through the EM strategy and segments the voxels by MAP in an interleaved manner between labels and mixtures, converging to a solution where the model parameters and voxel labels are stabilized within a specified criterion.

Let $Y_i = \{Y_{il}\}_{l=1}^{L}$ be the intensity vector of L-channel MR images at location i over the 3-D image array of I voxels. Assume that the images consist of K classes (or tissue types) and each class k is characterized by a Gaussian parameter vector $\theta_k(\mu_k, \nu_k)$, i.e., the mean and variance. Let $p_k(Y_i|\theta_k)$ be the probability distribution of those voxel intensities that are associated with class k. We further assume that the multispectral MR images are statistically independent. The likelihood for each voxel Y_i, falling into K distinct classes, is then described by a finite multivariate functional as

$$g(Y_i|X, \Theta) = \sum_{k=1}^{K} p(k|X_{N_i}) p_k(Y_i|\theta_k) \tag{2}$$

where $p(k|X_{N_i})$ is the locally-dependent probability [15] of voxel label $X_i = k$. By the EM strategy, we have, at each iteration n

$$\mu_{kl}^{(n+1)} = \frac{\sum_i Z_{ik}^{(n)} Y_{il}}{\sum_i Z_{ik}^{(n)}} \tag{3}$$

$$\nu_{kl}^{(n+1)} = \frac{\sum_i Z_{ik}^{(n)} \left(Y_{il} - \mu_{kl}^{(n+1)}\right)^2}{\sum_i Z_{ik}^{(n)}} \tag{4}$$

where Z_{ik} is the conditional probability that voxel Y_i belongs to class k, which represents the tissue percentages within that voxel, i.e., it is the task of our mixture-based quantitative analysis [14]

$$Z_{ik}^{(n)} = \frac{p^{(n)}(k|X_{N_i}) \prod_{l=1}^{L} p\left(Y_{il}|\theta_k^{(n)}\right)}{\sum_j \left[p^{(n)}(j|X_{N_i}) \prod_{l=1}^{L} p\left(Y_{il}|\theta_j^{(n)}\right)\right]}. \quad (5)$$

If we ignore the local dependence of the voxel labels, $p(k|X_{N_i})$ becomes the weight of the finite multivariate function [7], [21]. Then the estimation of Z_{ik} becomes the maximum likelihood (ML) solution.

There are several ways to include the local dependence by specifying a function of $p(k|X_{N_i})$. A Markov random field (MRF) model is commonly used to reflect the neighborhood information [11], [22]. An energy function $U(X)$ is constructed to specify the degree of penalty imposed on the neighbors, and can be defined, in three dimensions, as

$$U(X) = \sum_{i=1}^{N} \left\{ \sum_{r \in c_i^1} [1 - \delta(X_i - X_r)] + \sum_{s \in c_i^2} [1 - \delta(X_i - X_s)] \Big/ \sqrt{2} \right\} \quad (6)$$

where $\delta(0) = 1$, $\delta(\neq 0) = 0$. The index r runs over the six first-order neighbors and s runs over the 12 second-order neighbors. The assignment of labels over the voxel array is performed by the MAP criterion.

E. Extraction of the CCA

Besides the quantitative analysis of WM and GM brain tissues, a quantitative measure of cerebral atrophy (CA) was also assessed in this study. CA has been shown to correlate with a variety of cognitive functions, including those functions most commonly disturbed. It may represent the final cumulative effect of different types of MS induced lesions [23]. In the segmented mixture image or mixels, by choosing a central CSF seed, the central CSF volume was delineated by both morphology and region growing technologies. In some datasets where the central CSF and peripheral CSF are connected, these connections could induce an overestimation of the central CSF. Therefore, a user-friendly semi-automated tool was developed to assist the physicians to appropriately cut the connections between the central and peripheral CSFs. In clinic studies, lesions appear in patient datasets with the same intensity feature as CSF in both T_1- and T_2-weighted images. Therefore, FLAIR images, where lesion intensity appears brighter than those of other tissues, were acquired to detect the lesions. Small lesions or low probability lesions were eliminated first. Flair image artifacts, which are easily distinguished after segmentation, were eliminated through the semi-automatic tool. Then, the detected lesions were subtracted from the segmented CSF result to minimize the error for atrophy measure. In this study, we proposed the following definitions for quantitative validation:

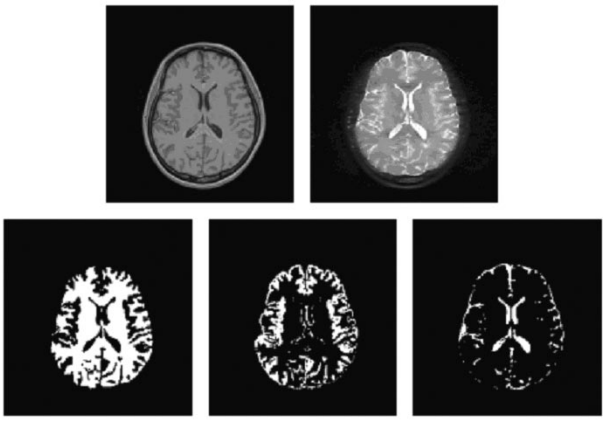

Fig. 2. The T_1-, T_2-weighted MR images (top) and the extracted WM, GM, and CSF (bottom).

1) ICV = WM + GM + total CSF;
2) WM fraction (WMF) = WM/ICV;
3) GM fraction (GMF) = GM/ICV;
4) total atrophy (TA) = total CSF/ICV;
5) CCA = central CSF/ICV;
6) peripheral atrophy (PA) = peripheral CSF/ICV.

F. Evaluation Methods

We evaluated the accuracy and repeatability of the MAP-EM framework through phantom, healthy volunteer and patient studies. In the patient studies, the correlations with radiologists' rating and neurologists' scoring were performed. The accuracy were assessed using both the mathematical brain phantom images downloaded from the Connell Brain Imaging Center, McGill University, Montreal, Canada, and a physical brain phantom, where the gold standards are known. Repeatability was assessed by performing our MAP-EM segmentation scheme on a series of images from both phantoms and healthy volunteers, under the assumption that the phantom and healthy volunteer brains would not change during the evaluation period. Repeatability was assessed by calculating the following:

$$\text{Repeatability} = \text{standard deviation (stdev)}/\text{mean}.$$

III. Results and Discussion

A. Visual Evaluation

Fig. 2 shows the original T_1- and T_2-weighted images from a volunteer study and the corresponding MAP-EM segmented labels indicating WM, GM, and CSF (quantitative measures on mixtures is reported below). A 3-D surface rendering of the extracted central CSF from one subject as viewed from two different angles is shown in Fig. 3.

The total computing time of this algorithm for the results was approximately 25 min for a set of multispectral images with $256 \times 256 \times 160$ size on a PC/800 Mhz Pentium III.

B. Quantitative Evaluation

1) Mathematical Phantom Studies: The presented segmentation scheme is fully automated except for the separation of

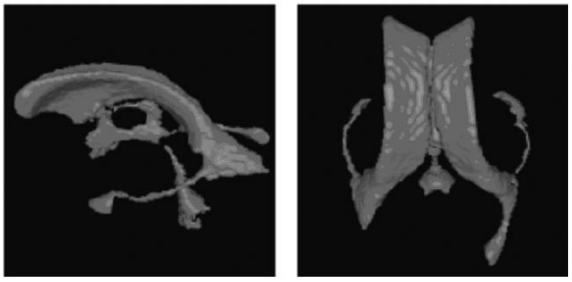

Fig. 3. The 3-D surface rendering of the extracted central CSF from one subject as viewed from two different angles.

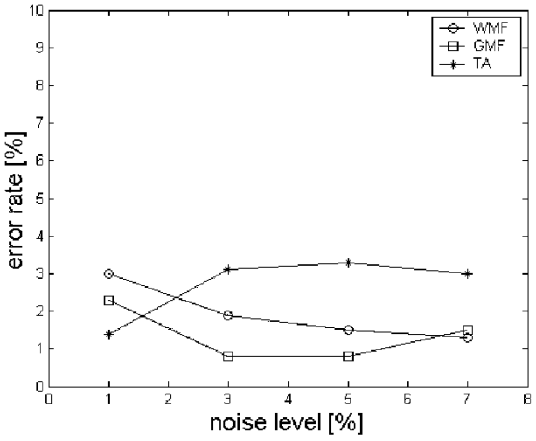

Fig. 4. Error rate of the mixture-based quantitative estimation of brain tissues at different noise levels.

central and peripheral CSF's. Therefore, quantitative estimation of WM, GM, and total CSF is 100% reproducible.

For the phantom images of the anatomical models from the Connell Brain Imaging Center, McGill University, the total volumes of CSF, GM, and WM are given as 371.9, 902.9, and 674.8 (cm3), respectively. Therefore, the ICV volume is 1949.6 (cm3). We used the Brainweb MRI simulator to generate a series of six scans/images based on the mathematical brain phantom with 1 mm cubic voxel size at different noise levels. The nonuniformity effect of image density in this study was set to 0%. Fig. 4 demonstrates the accuracy of the mixture-based quantitative estimation of brain tissues at different noise levels, where the region to cover a mixture component is given by the corresponding labeled area. The repeatability test on the phantom studies at different noise levels is shown in Fig. 5. The accuracy and repeatability of the algorithm are satisfactory.

2) Physical Phantom Studies: A brain phantom was constructed by plastic materials with three compartments of WM, GM, and CSF filled with different concentrations of Gadolinium (Gd) contrast solution. From the brightest to darkest intensities in the T_1-weighted image of Fig. 6(a), it contains 6 mM, 1 mM, 0.1 mM Gd solutions, respectively. From the largest to smallest size, the diameters of the cylinders are 97.5 mm, 37.5 mm (with wall thickness 3 mm), and 28.5 mm (with wall thickness 1.8 mm), respectively. The physical phantom was scanned by our 1.5 Tesla whole body MRI scanner using the protocol as described above. Five scans were performed in five weeks, i.e., one scan per week.

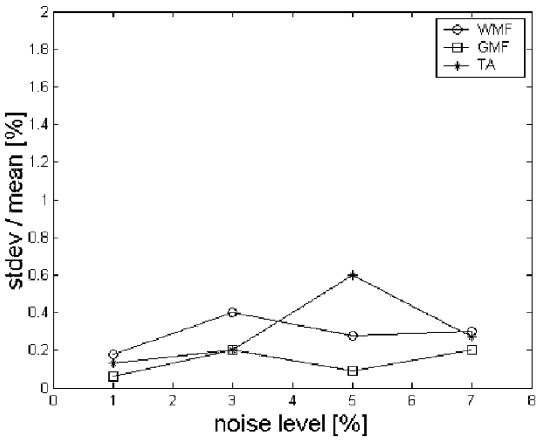

Fig. 5. Repeatability test on the phantom images at different noise levels.

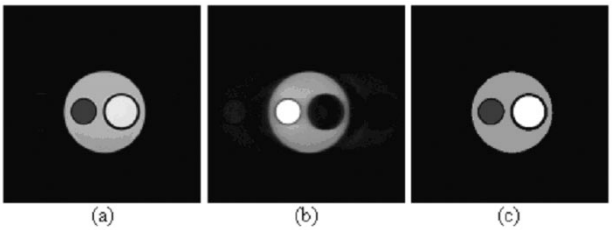

Fig. 6. One of the image planes from the physical phantom dataset. (a) T_1-weighted image. (b) T_2-weighted image. (c) Segmented image.

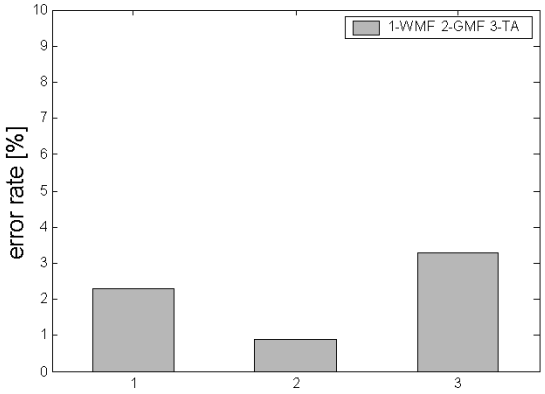

Fig. 7. Quantitative error rate of estimating different volumes on physical phantom studies.

Fig. 6 shows one slice of a volume scan from the physical phantom (T_1- and T_2-weighted images) and the corresponding segmented image. Accuracy and repeatability studies on the physical phantom are shown in Fig. 7 and Fig. 8, respectively. The error rate is less than 3.3% and the repeatability is below 0.1%.

3) Volunteer Studies: Two volunteers (age 33, one male and one female) were recruited in this evaluation study. Four scans were performed within one year for each volunteer.

For healthy volunteers, only repeatability test was assessed. Fig. 9 shows the repeatability test on the two volunteer studies, each having a series of four scans. The CCA measurements have achieved a high repeatability with less than 1.9%, indicating the feasibility of our segmentation scheme for neurological diagnosis and follow up evaluation on MS. Other measurements of

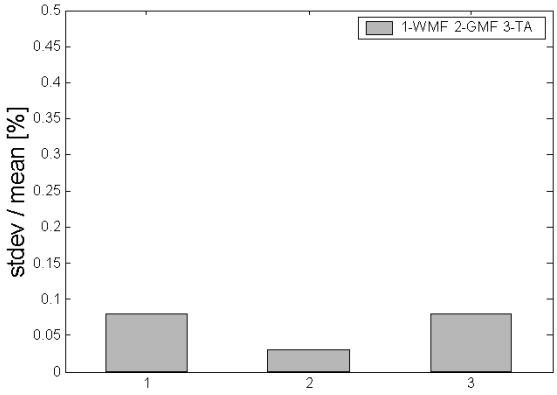

Fig. 8. Repeatability test on physical phantom studies.

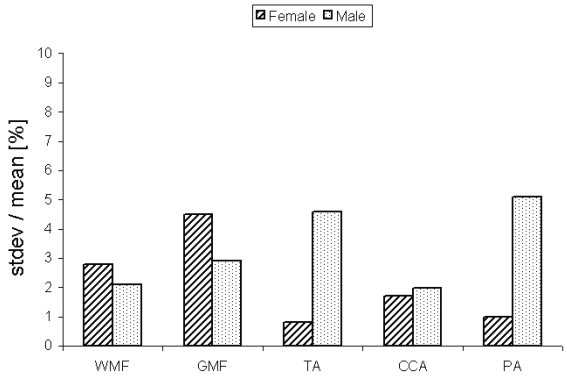

Fig. 9. Repeatability test of volumetric analysis on volunteer studies.

WM, GM, total CSF, and peripheral CSF have an average variation of around 2.5%.

It should be noted that for the phantom studies, the gold standards are known, so both the accuracy and repeatability tests do not have the problem of image registration. However, for the volunteer studies, the registration of the series images can be a problem for quantitative measures. In our quantitative analysis framework, we assume that the skull of an adult remains the same during the time period. Based on this assumption, the ICVs of each subject in the series scans become the relative references for those scans. Therefore, the ratios on each relative reference, respectively, have the spatial invariant property, eliminating the registration problem. In Fig. 9, the variation of the ICV causes a noticeable change for the brain tissues, but the ratios minimize the variation.

4) Patient Studies:

a) Validation of the CCA Volumetric Analysis and Total Lesion Load (TLL): Seven MS patients (age range of 20–55 years old) were recruited for this validation study. The patients were clinically described as relapsing remitting and secondary progressive MS patients. For all patients, multispectral images of 1.5 mm slice-thickness were acquired, as described above. Each patient was scanned twice [baseline (BL) and half-year (HY) scans] with a half-year interval within one year, resulting in a total of 14 datasets. The quantitative measurements (cm3) and TLL from our MAP-EM segmentation of these patients' datasets are listed in Table I, where the segmentation results are

TABLE I
QUANTITATIVE MEASUREMENTS (cm3) FROM PATIENTS' DATASETS

Subject	WM	GM	CSF	CCSF	CCA	TLL
1(BL)	779.02	470.44	280.27	16.33	1.07	0.87
1(HY)	788.77	501.32	248.62	17.04	1.11	1.14
2(BL)	710.24	456.27	291.71	15.28	1.05	1.31
2(HY)	693.01	520.27	252.33	17.19	1.17	5.21
3(BL)	749.25	478.7	325.86	31.74	2.04	3.35
3(HY)	723.84	494.62	332.16	33.61	2.16	3.46
4(BL)	697.18	508.60	296.65	21.44	1.42	1.58
4(HY)	759.71	480.51	286.12	21.87	1.43	1.10
5(BL)	600.56	515.62	234.69	20.72	1.53	0.14
5(HY)	545.62	561.08	239.60	21.42	1.59	0.95
6(BL)	670.95	412.56	278.03	62.43	4.58	1.50
6(HY)	654.01	386.46	305.46	64.44	4.78	1.99
7(BL)	673.42	395.73	226.49	57.66	4.41	12.26
7(HY)	637.45	374.71	234.58	57.80	4.57	15.55

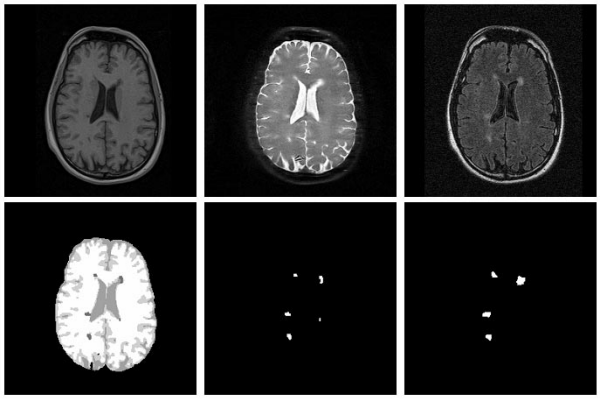

Fig. 10. One slice of the T_1-, T_2-weighted, FLAIR images (top), the segmented image (bottom left), the MS lesion classification (bottom middle), and the radiologist's delineation of the MS lesions (bottom right).

shown in Fig. 10. The CCA has been found to have particularly high rates of increase per year in longitudinal MS studies [24]. Development of MS disease is consistently seen within a half-year period for each subject.

A user-friendly computer interface was developed for radiologists to manually trace and delineate the MS lesions on the FLAIR images as the gold standard. It is noted, due to the limited quality of the FLAIR images, the manually drawn lesion volumes from FLAIR images have a variation with our segmented results from the corresponding multispectral images. This can be clearly seen from Fig. 10. With improved quality of FLAIR images, the variation is expected to be smaller. Nevertheless, the detection of lesions by our MAP-EM framework is consistent with the radiologists' findings.

b) Correlation of the CCA Analysis With Clinical Measures: In order to validate the feasibility of the CCA analysis for MS burden, three radiologists rated independently the amount of CCA on the MRI films of eight MS patients with cognitive impairment. The rating scale was from one to nine, corresponding to the following labels: small(−), small, small(+), medium(−), medium, medium(+), large(−), large, large(+). The correlation between our volumetric measure and radiologists' CCA rating is shown in Fig. 11. The correlation is very strong, ranging from $r = 0.957$ to $r = 0.982$ (all

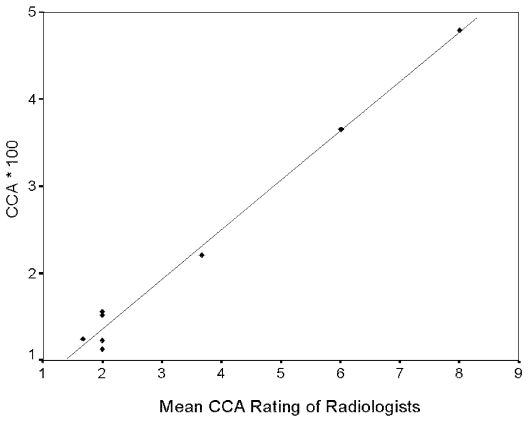

Fig. 11. Correlation of MAP-EM CCA measures and radiologists' CCA ratings.

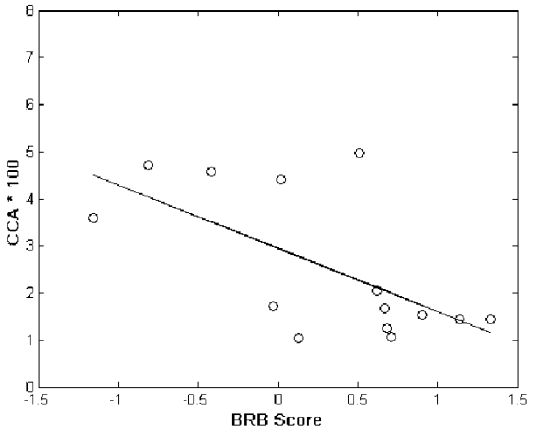

Fig. 12. Correlation of MAP-EM CCA measure and neurologists' BRB composite scoring.

significant at $p \leq 0.000$). It is noted that this study is based on an average of radiologists' subjective judgments. A slight bias is observed due to subjective ratings and limited sample size, as shown in Fig. 11.

In addition, the correlation between our MAP-EM CCA measure and the neurologists' BRB composite scoring for a sample of 14 patients (including the 8 patients above) was studied. The result is shown in Fig. 12. A strong correlation is again seen with $r = 0.622$ and $p = 0.013$ in overall cognitive performance.

IV. Conclusion

We developed and validated our mixture-based segmentation algorithm with inclusion of noise reduction as well as PSF analysis for resolution enhancement. The initial estimate for the iterative MAP-EM update is given by the SOVQ scheme [20]. The iterative convergence is guaranteed by the MRF model. Therefore, the algorithm is fully automated with 100% reproducibility on quantitative estimation of WM, GM, and CSF except for the separation of central and peripheral CSFs. The segmentation of tissue mixtures, rather than voxel label, is an optimal solution for minimizing the PVE. Both digital and physical phantom studies demonstrated satisfactory accuracy and repeatability. Preliminary studies on patient datasets showed the consistence on MS development in a one-year period. Strong correlations of our MRI volumetric measure with radiologists' rating and neurologists' BRB scoring were seen and consistent with the clinical findings [12].

The validation on accuracy and repeatability reflects the feasibility of our MRI volumetric framework for quantitative analysis of MS as an accepted clinical tool. Further research on improving the analysis with inclusion of inter and intraslice in-homogeneity correction is under progress [25].

Acknowledgment

The authors wish to thank radiologists, C. Roque, R. Peyster, and P. Roche for supplying CSF rating and their manually drawn lesions for this work.

References

[1] S. L. Hauser, "Multiple sclerosis and other demyelinating diseases," in *Harrison's Principles of Internal Medicine*, 13th ed. New York: McGraw-Hill, 1994, pp. 2287–2295.

[2] J. F. Kurtzke and M. Wallin, "Multiple sclerosis: Diagnosis, medical management, and rehabilitation," in *Epidemiology*, J. S. Burks and K. P. Johnson, Eds: New York, 2000, pp. 49–71.

[3] R. A. Rudick, E. Fisher, J. C. Lee, J. Simon, L. Jacobs, and the MS Collaborative Research Group, "Use of brain parenchymal fraction to measure whole brain atrophy in relapsing remitting MS," *Neurol.*, vol. 53, pp. 1698–1704, 1999.

[4] D. Chen, W. Huang, C. Christodoulou, L. Li, H. Qian, L. Krupp, and Z. Liang, "A new method for quantitative analysis of multiple sclerosis using MR images," *SPIE Med. Imaging*, pp. 375–380, 2001.

[5] E. M. Haacke, R. W. Brown, M. R. Thompson, and R. Venkatesan, *Magnetic Resonance Imaging: Physical Principles and Sequence Design*. New York: Wiley, 1999.

[6] M. A. Brown and R. C. Semelka, *MRI: Basic Principles and Applications*. New York: Wiley, 1995.

[7] Z. Liang, J. R. MacFall, and D. P. Harrington, "Parameter estimation and tissue segmentation from multispectral MR images," *IEEE Trans. Med. Imaging*, vol. 13, pp. 441–449, 1994.

[8] K. V. Leemput, F. Maes, D. Vandermeulen, A. Colchester, and P. Suetens, "Automated segmentation of multiple sclerosis lesions by model outlier detection," *IEEE Trans. Med. Imaging*, vol. 20, pp. 677–688, Aug. 2001.

[9] B. Johnston, M. S. Atkins, B. Mackiewich, and M. Anderson, "Segmentation of multiple sclerosis lesions in intensity corrected multispectral MRI," *IEEE Trans. Med. Imaging*, vol. 15, pp. 154–169, Apr. 1996.

[10] A. P. Zijdenbos, B. M. Dawant, R. A. Margolin, and A. C. Palmer, "Morphometric analysis of white matter lesions in MR images: Method and validation," *IEEE Trans. Med. Imaging*, vol. 13, pp. 716–724, Dec. 1994.

[11] K. Held, E. R. Kops, B. J. Krause, W. M. Wells, R. Kikinis, and H. Muller-Gartner, "Markov random field segmentation of brain MR images," *IEEE Trans. Med. Imaging*, vol. 16, pp. 878–886, Dec. 1997.

[12] W. Huang, C. Christodoulou, L. Li, A. Tudorica, X. Li, P. Roche, W. Scheri, R. Peyster, C. Roque, P. Melville, V. Geronimo, Z. Liang, and L. Krupp, "Correlation studies of multiple sclerosis using 1H MRS, volumetric MRI, and cognitive test," in *Proc. Int. Soc. Magn. Resonance Med.*, vol. 1, 2002, p. 595.

[13] D. Miller, R. Grossman, S. Reingold, and H. McFarland, "The role of magnetic resonance techniques in understanding and managing multiple sclerosis," *Brain*, vol. 121, pp. 3–24, 1998.

[14] L. Li, X. Li, W. Huang, C. Christodoulou, D. Chen, A. Tudorica, P. Djuric, L. Krupp, and Z. Liang, "A novel mixture-based segmentation algorithm for quantitative analysis of multiple sclerosis using multispectral MR images," in *Proc. Int. Soc. Mag. Resonance Med.*, vol. 1, 2002, p. 354.

[15] Y. Zhang, M. Brady, and S. Smith, "Segmentation of brain MR images through a hidden Markov random field model and the expectation-maximization algorithm," *IEEE Trans. Med. Imaging*, vol. 20, pp. 45–57, Jan. 2001.

[16] Z. Liang, J. Ye, J. Cheng, and D. P. Harrington, "The inversion of the exponential Radon transform for quantitative brain SPECT," *Phys. Medicine Biol.*, vol. 41, pp. 1227–1232, 1996.

[17] D. L. Parker and G. T. Gullberg, "Signal-to-noise efficiency in magnetic resonance imaging," *Med. Phys.*, vol. 17, pp. 250–257, 1990.

[18] H. Lu, X. Li, I. Hsiao, and Z. Liang, "Analytical noise treatment for low-dose CT projection data by penalized weighted least-square smoothing in the K–L domain," *SPIE Med. Imaging*, vol. 4682, pp. 146–152, 2002.

[19] J. Ye, Z. Liang, and D. P. Harrington, "Quantitative reconstruction for myocardial perfusion SPECT: An efficient approach by depth-dependent deconvolution and matrix rotation," *Phys. Medicine Biol.*, vol. 39, pp. 1263–1279, 1994.

[20] L. Li, D. Chen, H. Lu, and Z. Liang, "Segmentation of MR brain images: A self-adaptive online vector quantization approach," *SPIE Med. Imaging*, vol. 4322, pp. 1431–1438, 2001.

[21] Z. Liang, R. J. Jaszczak, and R. E. Coleman, "Parameter estimation of finite mixtures using the EM algorithm and information criteria with application to medical image processing," *IEEE Trans. Nucl. Sci.*, vol. 39, pp. 1126–1133, Aug. 1992.

[22] R. Leahy, T. Hebert, and R. Lee, "Applications of Markov random fields in medical imaging," *Inform. Processing Med. Imaging*, pp. 1–14, 1991.

[23] W. J. Jagust, "Brain atrophy as a surrogate marker in MS: Faster, simpler, better?," *Neurol.*, pp. 782–783, 2000.

[24] J. H. Simon, "Brian and spinal cord atrophy in multiple sclerosis," *Neuroimaging Clinics North America*, vol. 10, pp. 753–769, 2000.

[25] D. Chen, L. Li, D. Yoon, J. H. Lee, and Z. Liang, "A renormalization method for inhomogeneity correction of MR images," *SPIE Med. Imaging*, vol. 4322, pp. 939–942, 2001.